SCIENTIFIC REPORTS
nature research

OPEN

First-principles investigation of the ferroelectric, piezoelectric and nonlinear optical properties of $LiNbO_3$-type $ZnTiO_3$

Jing Zhang[1*], Bin Xu[1], Yu-Sheng Wang[1], Zhen Qin[1] & San-Huang Ke[2]

The newly synthesized LN-type $ZnTiO_3$ (J. Am. Chem. Soc. 2014, 136, 2748) contains cations with the electronic configurations nd^{10} (Zn^{2+}: $3d^{10}$) along with second-order Jahn-Teller (SOJT) nd^0 (Ti^{4+}: $3d^0$) cations. This is different from traditional ferroelectrics with the electric configurations of d^0 transition metal ions or/and lone pair electrons of ns^2. Using a first-principles approach based on density functional theory, we investigate the electronic structure, zone-center phonon modes, piezoelectric and nonlinear optical properties of the $LiNbO_3$-type $ZnTiO_3$. The electronic structure indicates that this compound is a wide direct-band-gap insulator. The results reveal that this compound is a good ferroelectric material with a large spontaneous polarization of 90.43μC/cm². The Raman scattering peaks of A_1 and E modes are assigned to their zone-center optical modes. Additionally, the large piezoelectric and nonlinear optical susceptibilities reveal that $LiNbO_3$-type $ZnTiO_3$ is a high-performance lead-free piezoelectric and nonlinear optical crystal.

In recent years, noncentrosymmetric (NCS) compounds have attracted great interest in physics and material science because of their symmetry-dependent ferroelectric, piezoelectric and second-order nonlinear optical (NLO) properties, etc[1,2]. When searching for other polar oxides, researchers pay special attention to two classes of compounds, specifically those that include second-order Jahn-Teller distorted (SOJT) cations (Te^{4+}, Sn^{4+} Ti^{4+}, Mo^{6+}, Nb^{5+}, V^{5+}, etc.) and cations with stereoactive lone pair electrons of ns^2 (Bi^{3+}, Pb^{2+}, Se^{4+}, etc.)[3–12]. For the NCS compounds, there are two famous structures: perovskite-type (Pv-type) and $LiNbO_3$-type (LN-type) phases. Taking into account the structural relationship between the above two, the $LiNbO_3$-type structure can be regarded as the derivative of the perovskite structure[13]. In general, most of the LN-type compounds cannot be synthesized under general conditions and instead require high temperature and high pressure.

In 2014 a new NCS compound, the LN-type $ZnTiO_3$, was synthesized by Inaguma *et al.* under high temperature and high pressure[14]. Their results show that LN-type $ZnTiO_3$ has a large spontaneous polarization and greater second harmonic generation (SHG) response compared to $LiNbO_3$ and LN-type $ZnSnO_3$. According to Bartram *et al.*[15], Ito *et al.*[16] and Inaguma *et al.*'s reports[14], two paraelectric phases of $ZnTiO_3$ are ilmenite (IL)-type (hexagonal space group $R\bar{3}$) and Pv-type (orthorhombic space group Pnma) structures, respectively. Ito *et al.* reported that IL-type $ZnTiO_3$ decomposes into ZnO and TiO_2 under a pressure of 20∼25 GPa[16]; inspired by this, Inaguma *et al.* successfully synthesized LN-type $ZnTiO_3$ at less than 20 Gpa. As discussed by Navrotsky[13] and Linton *et al.*[17], the LN-type compounds such as $ZnSnO_3$, $FeTiO_3$, $MnTiO_3$ and $ZnGeO_3$, etc. are metastable and quenched products from the high-pressure perovskite phases[18–24]. This means that LN-type $ZnTiO_3$ is regarded as a retrograde product from the high-pressure perovskite phase on pressure release[14]. The crystal structures of $ZnTiO_3$ in the ferroelectric and two paraelectric phases are presented in Figs. 1 and 2, respectively.

Notice that recently-synthesized LN-type $ZnSnO_3$ and $CdPbO_3$ are novel polar oxides (hexagonal space group R3c) that include only the cations with the electronic configurations of nd^{10} (Zn^{2+} $3d^{10}$, Cd^{2+} $4d^{10}$, Sn^{4+} $4d^{10}$, Pb^{4+} $5d^{10}$) and provide a new strategy for synthesizing new polar compounds. The LN-type $ZnTiO_3$ contains not only Zn^{2+} ($3d^{10}$), but also Ti^{4+} ($3d^0$), the former and later belonging to nd^{10} and SOJT nd^0 cations, respectively. Although LN-type $ZnTiO_3$ and $ZnSnO_3$ have the similar crystal structures, experimental results have shown

[1]School of of Physics and Electronics, North China University of Water Resources and Electric Power, ZhengZhou, 450045, China. [2]School of Physics Science and Engineering, Tongji University, 1239 Siping Road, Shanghai, 200092, P.R. China. *email: zhangjing@ncwu.edu.cn

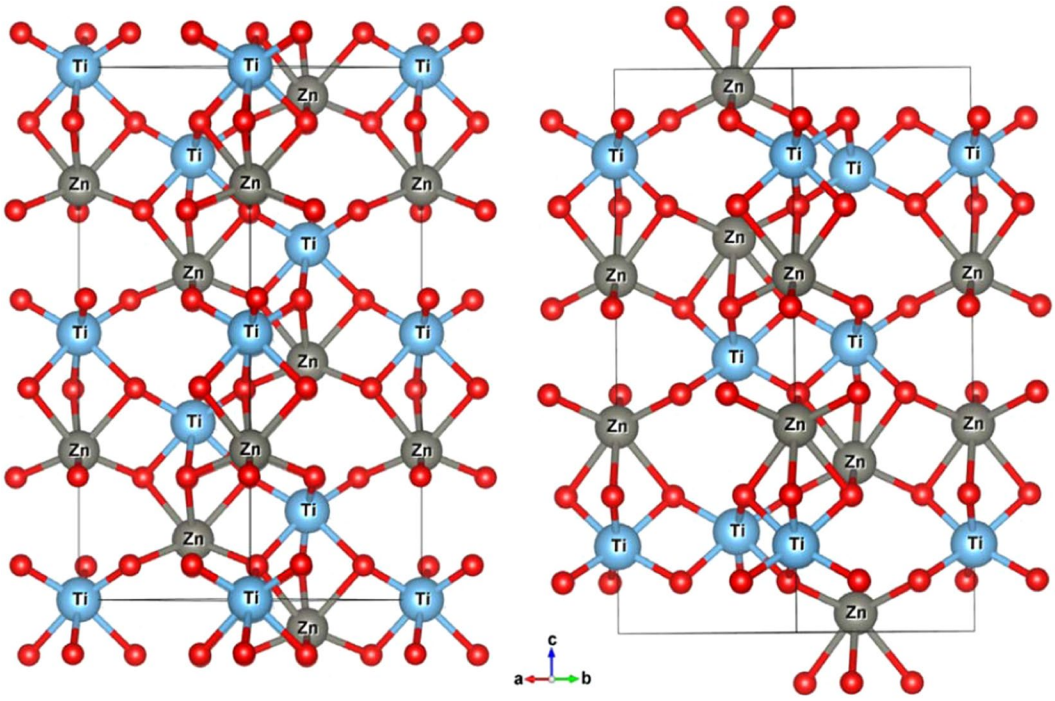

Figure 1. The crystallographic structures of $LiNbO_3$ (LN)-type $ZnTiO_3$ (left, space group R3c) and ilmenite (IL)-type $ZnTiO_3$ (right, space group $R\bar{3}$) along the z-axis.

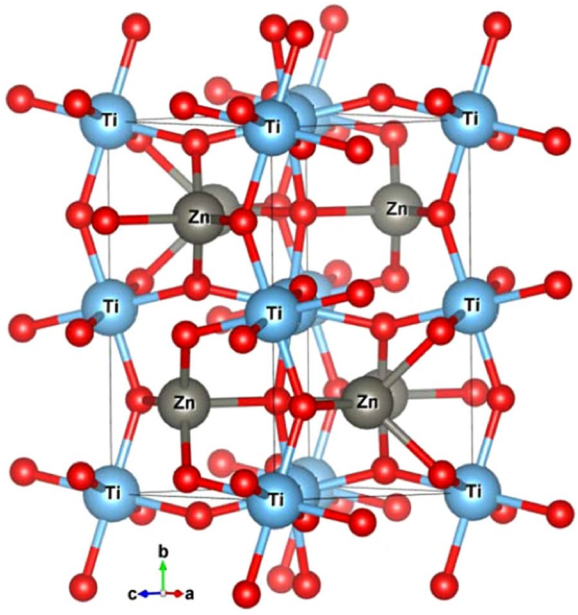

Figure 2. A view of the crystal structure of perovskite(Pv)-type $ZnTiO_3$ (space group Pnma) along the y-axis.

that the SHG intensity of LN-type $ZnTiO_3$ is 24 times greater than that of LN-type $ZnSnO_3$[14]. The space group of LN-type $ZnTiO_3$ belongs to the 3 m polar point group, so this compound is a promising candidate as a piezoelectric and nonlinear optical material. Therefore, LN-type $ZnTiO_3$ provides a perfect example for comparing the influence that the nd^{10} and SOJT nd^0 cations have in producing the ferroelectric, piezoelectric and nonlinear optical behavior.

Nowadays, first-principles calculations based on density functional theory (DFT) play an important role in meeting the needs of experimenters because they can accurately predict the properties of new materials at the atomic scale. In general, the measurements of piezoelectric and nonlinear optical properties require very high crystal quality, specialized laboratories, and are expensive, so first-principles calculations provide an alternative to predicting optical and piezoelectric properties, and can be microscopically explain the relationship between

structure and properties. First-principles calculations including the modern theory of polarization[25,26], linear corresponding approaches, as well as the density functional perturbation theory (DFPT)[27–29], can help us study the ferroelectric, piezoelectric, and nonlinear optical properties of materials. In addition to traditional ferroelectrics, first-principles calculations have made great progress in predicting and investigating new nonlinear optical crystal[30,31], multiferroic materials[32,33], two-dimensional ferroelectrics[34] and ferroelectric metal[35,36], etc. In order to study the intrinsic correlation from the paraelectric to ferroelectric phase transition, we have investigated the zone-center phonon modes of the ilmenite, perovskite and $LiNbO_3$-type $ZnTiO_3$ phases, respectively. Additionally, there have been no prior reports on the piezoelectric and nonlinear optical properties, including nonlinear optical susceptibilities and electro-optical coefficients, of LN-type $ZnTiO_3$, and so in this paper we carry out first-principles calculations to investigate the origin of the ferroelectric behavior, and analyze the piezoelectric and nonlinear optical properties of LN-type $ZnTiO_3$ for the first time. Since the piezoelectric and nonlinear optical properties of this type of novel material with nd^{10} and SOJT nd^0 cations have not been investigated previously, our calculations provide an important complement to experimental research.

Method

Our calculations are based on the framework of density functional theory (DFT). We mainly used the ABINIT package[37,38]. In order to calculate the electronic structure, spontaneous polarization, zone-center phonon modes, piezoelectric and nonlinear optical properties, we adopt norm-conserving pseudopotentials based on the local density approximation (LDA) as exchange-correlation potentials. An $8 \times 8 \times 8$ Monkhorst-Pack k-point mesh is used with a plane wave cut-off of 45 hartrees. The Zn 3d, 4s and Ti 3d, 4s, as well as O 2s, 2p electrons are regarded as valence states to construct the pseudopotentials. The electronic structures are also calculated by adopting ultrasoft pseudopotentials[39] based on the Vienna ab initio simulation package (VASP)[40–42], and the exchange-correlation potentials are based on LDA and the general gradient approximation (GGA) with Perdew-Burke-Ernzerhof (PBE) functional[43,44], respectively. Additionally, due to DFT systematically underestimate band gaps with respect to experiment, the Heyd-Scuseria-Ernzerhof (HSE) screened hybrid functional (with the version HSE06)[45,46] is used to calculated the band structures.

The calculations of the polarization and piezoelectric properties are based on linear response functions, while the computations of nonlinear optical properties are based on nonlinear response functions. The linear and nonlinear response calculations are performed using density functional perturbation theory (DFPT). In order to calculate the above physical properties, the homogeneous electric fields, atomic displacements and stresses are regarded as perturbations. When stress is applied to a piezoelectric crystal, its interior will produce a polarization phenomenon where opposing positive and negative charges appear on its two opposite surfaces. This phenomenon is called the positive piezoelectric effect. On the contrary, when the electric field is applied in the polarization direction of the piezoelectric crystal, it will also deform. After the electric field is removed, the deformation of the piezoelectric crystal disappears. This phenomenon is called the reverse piezoelectric effect. In this work, we calculate the piezoelectric stress tensor from the zero-field derivative of polarization by using stress as a perturbation:

$$e_{\alpha i} = \left.\frac{\partial p_\alpha}{\partial \eta_i}\right|_E \tag{1}$$

where η and i represent second-rank stress tensor and the Cartesian coordinate direction. In the actual computation, the piezoelectric stress tensor comes from the response from fixed ions and relative displacement of the ions:

$$e_{\alpha i} = \left.\frac{\partial p_\alpha}{\partial \eta_i}\right|_\mu + \sum_k \frac{\partial p_\alpha}{\partial \mu_\alpha(k)} \frac{\partial \mu_\alpha(k)}{\partial \eta_i} \tag{2}$$

where μ represents the displacement of the ions. For an insulator, the relation between the polarization and macroscopic electric field can be described as follows:

$$P_i = P_i^s + \sum_{j=1}^{3} x_{ij}^{(1)} \varepsilon_j + \sum_{j,l=1}^{3} x_{ijl}^{(2)} \varepsilon_j \varepsilon_l + \ldots, \tag{3}$$

where P_i^s represents spontaneous polarization in zero electric field; $x_{ij}^{(1)}$ are linear dielectric constants, and $x_{ijl}^{(2)}$ are second-order nonlinear optical (NLO) coefficients. The NLO and electro-optic (EO) coefficients can be calculated from third-order energy derivatives within the $2n+1$ theorem[47]. Like $LiNbO_3$ and LN-type $ZnSnO_3$, we use the more convenient d tensor to represent NLO coefficients $x_{ijl}^{(2)}\left(d_{ijl} = \frac{1}{2} x_{ijl}^{(2)}\right)$. When applying an electric field to some crystals, especially piezoelectric crystals, their refractive index changes. This characteristic of a crystal can be described by refractive index ellipsoids. The phenomenon is known as the linear electro-optic (EO) effect or Pockels Effect:

$$\Delta\left(\frac{1}{n^2}\right)_i = \sum_{j=1}^{3} r_{ij} \varepsilon_j \tag{4}$$

where n and r_{ij} represent refractive index and linear EO coefficients (i = 1~6, and j = 1~3), respectively. Pockels effect exists only in the NCS crystals. The electro-optical (EO) tensor arises from the sum of three contributions: the electronic part, ionic contribution and piezoelectric effects[48,49].

$ZnTiO_3$ ($R\bar{3}$)	a (Å)	b (Å)	c (Å)	V (Å^3)
Expt ref. [15]	5.079	5.079	13.9270	311.1319
Present (LDA-NC)	5.0564	5.0564	13.9001	307.7801
Present (GGA-NC)	5.1647	5.1647	14.3519	331.5384
Present(GGA-PBEsol-NC)	5.1169	5.1169	14.1530	320.9172
$ZnTiO_3$ (Pnma)	**a (Å)**	**b (Å)**	**c (Å)**	**V (Å^3)**
Present (LDA-NC)	5.2026	7.4146	5.0631	195.3118
Present (GGA-NC)	5.3258	7.5722	5.18200	208.9797
Present(GGA-PBEsol-NC)	5.2751	7.4955	5.131523	202.8997
$ZnTiO_3$ (R3c)	**a (Å)**	**b (Å)**	**c (Å)**	**V (Å^3)**
Expt ref. [14]	5.09452(12)	5.09452(12)	13.7177(3)	308.332(12)
Present (GGA-NC)	5.2089	5.2089	13.9559	327.9307
Present (LDA-NC)	5.0878	5.0878	13.5610	304.0071
Present(GGA-PBEsol-NC)	5.1579	5.1579	13.7210	316.1275
Present (GGA- ultrasoft)	5.1384	5.1384	13.9478	318.9250
Present (LDA- ultrasoft)	5.0211	5.0211	13.5725	296.3407
Present (HSE06)	5.0678	5.0678	13.6395	303.3668

Table 1. The calculated Lattice constants and volumes of the ilmenite (IL)-type (space group $R\bar{3}$) and Perovskite (Pv)-type (space group Pnma) and $LiNbO_3$-type (space group R3c) $ZnTiO_3$ based on norm-conserving (NC), ultrasoft pseudopotentials and Heyd-Scuseria-Ernzerhof screened hybrid functional (HSE06).

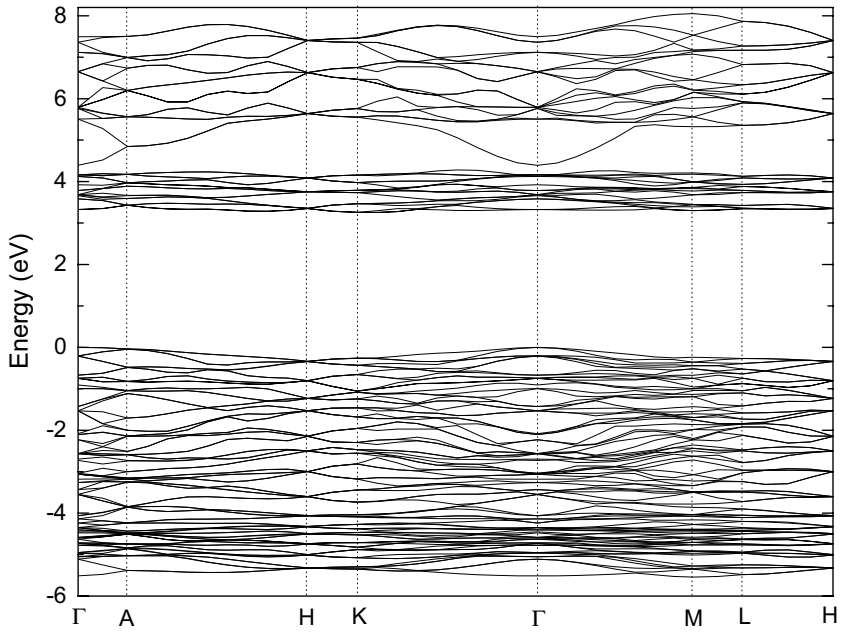

Figure 3. The band structures of $LiNbO_3$-type $ZnTiO_3$ along the high symmetry directions in the Brillouin zone based on norm-conserving pseudopotentials within GGA.

Results and Discussions

Electronic structure. Firstly, we perform the full geometry optimization to determine the crystal parameters in the paraelectric and ferroelectric phases. According to the optimized geometry (see Table 1), we have performed the electronic structure calculations of the $LiNbO_3$-type $ZnTiO_3$ based on ultrasoft and norm-conserving pseudopotentials and HSE06, respectively. Figures 3 and 4 plots the energy band structure of this compound along the high symmetry points in the first Brillouin zone based on norm-conserving pseudopotentials within GGA and HSE06. When calculating the energy band based on HSE06, more high symmetry points in the first Brillouin zone are used. From Fig. 3, it is found that the top of the valence band (VB) and the bottom of the conduction band (CB) are both located at Γ(0.0, 0.0, 0.0), so this compound is a direct band gap insulator. The calculated energy gaps (e_g) are as follows: 3.054 eV (LDA) and 3.252 eV (GGA) based on norm-conserving pseudopotentials; 2.860 eV (LDA) and 2.956 eV (GGA) based on ultrasoft pseudopotentials. Therefore, the energy gap of norm-conserving pseudopotentials is slightly larger than that of ultrasoft pseudopotentials. From Fig. 4, it is found that the e_g based on HSE06 (see in Fig. 4) are 4.25 eV. So, the band gap based on HSE06 is the largest

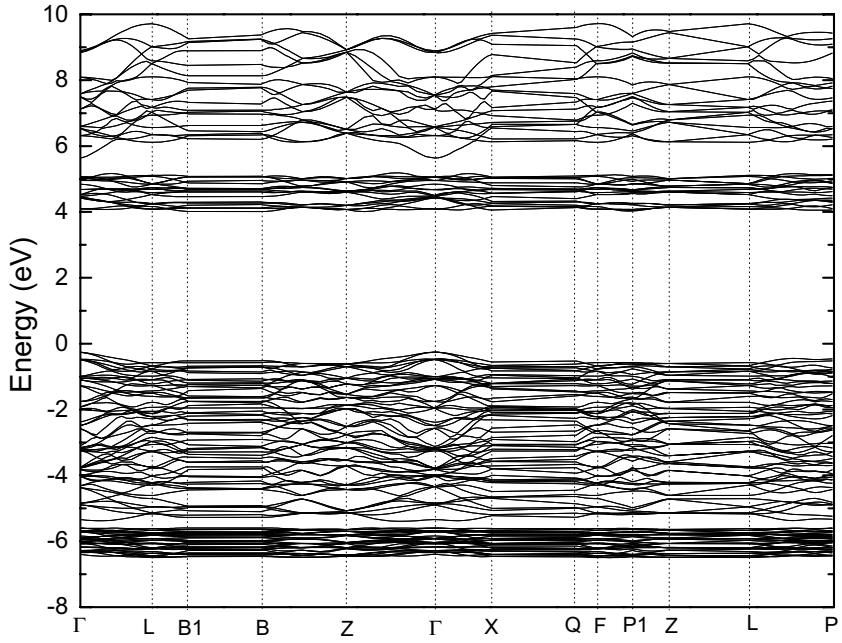

Figure 4. The band structures of $LiNbO_3$-type $ZnTiO_3$ along the high symmetry directions in the Brillouin zone based on HSE06.

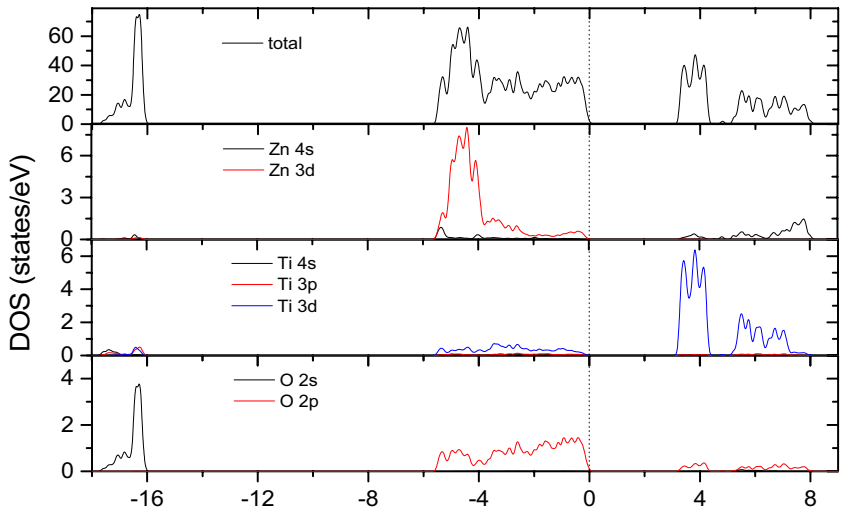

Figure 5. Total and partial density of states (DOSs) of LN-type $ZnTiO_3$ based on norm-conserving pseudopotentials within GGA with the Fermi levels at 0 eV.

and is about 1 eV higher than that of GGA based on norm-conserving pseudopotentials. From Table 1, one can see that the lattice parameters of LDA and GGA are slightly lower and higher than the experimental values. The difference in the band gaps between GGA and LDA result from the difference in calculated lattice parameters. Compared with the results of LDA and GGA, the lattice parameters based on HSE06 are the lowest, however the band gap is the largest. Until now,as far as we know there is no experimental report on the band gap of LN-type $ZnTiO_3$. Although the band gap of HSE06 is relatively larger than that of LDA and GGA, the agreement with the experimental band gap needs further verification.

Figure 5 shows the total and partial density of states (DOSs) of LN-type $ZnTiO_3$ based on norm-conserving pseudopotentials within GGA. According to this figure, in the energy region from −18 to −16 eV, the total DOS mainly arises from O 2p electrons, with a small contribution from Zn 4s electrons and Ti 3p, 3d and 4s electrons. In the energy range from −6 to −0 eV, the total DOS mainly arises from Zn 3d, Ti 3d and O 2s electrons, and there are obviously hybridizations between Zn 3d-O 2p and Ti 3d-O 2p states. Above the Fermi level, in the range 3 to 8 eV, the total DOS mainly arises from Ti 3d, Zn 3d and O 2p electrons. The calculated Mulliken charge populations of this compound are as follows: for Zn atom, the charge populations of the s, p and d orbitals are 0.27, 0.70 and 9.98; for Ti atom, the charge population of the s, p and d orbitals are 2.37, 6.43 and 2.15; for O atom,

Atom	Z_{xx}^*	Z_{yy}^*	Z_{zz}^*	Z_{xy}^*	Z_{yx}^*	Z_{xz}^*	Z_{zx}^*	Z_{yz}^*	Z_{zy}^*
Zn	2.59	2.59	2.29	0.24	−0.24	0.00	0.00	0.00	0.00
Ti	6.16	6.16	5.34	−0.54	0.54	0.00	0.00	0.00	0.00
O_1	−2.19	−3.64	−2.54	−0.58	−0.55	−0.31	−0.35	−1.28	−1.32
O_2	−3.77	−2.06	−2.54	−0.35	−0.34	1.27	1.32	0.37	0.37
O_3	−2.79	−3.04	−2.54	0.90	0.92	−0.96	−0.97	0.91	0.95

Table 2. The calculate Born effective charge of Zn, Ti, $O_{1\sim3}$ in LN-type $ZnTiO_3$.

the charge populations of the s and p orbitals are 1.85 and 4.85. In addition, the calculated charge populations between nearest-neighboring (1.8652 Å) and next nearest-neighboring (2.1589 Å) Ti-O bonds are 0.56 and 0.30; the charge populations between the nearest-neighboring (2.0421 Å) and next nearest-neighboring (2.2671 Å) Zn-O bonds are only 0.29 and 0.04. The number of charges on the different bonds can reflect the covalent and ionic properties. Obviously, the chemical bonding of the Ti-O and nearest-neighboring Zn-O bonds are of mixed covalent-ionic character, however the next nearest-neighboring Zn-O bonds show ionic character. As discussed above, the hybridization of Zn-O bonds and Ti-O bonds mainly occurs in their 3d and 2p orbitals. The charge distribution of Zn-O and Ti-O bonds indicates that the empty 3d orbital in Ti^{4+} ($3d^0$) more easily forms a covalent bond with O atoms than the fully occupied 3d orbital in Zn^{2+} ($3d^{10}$). This may be the reason why the piezoelectric and nonlinear optical properties of LN-type $ZnTiO_3$ are superior to those of the LN-type $ZnSnO_3$ and LN-type $ZnGeO_3$ (see the results below). In the latter two compounds, it is noted that the all the cations are fully occupied 3d orbitals.

Spontaneous polarization. The most basic characteristics of ferroelectric materials is the existence of spontaneous polarization over certain temperature ranges, and the fact that the polarization can be reversed by the external electric field. Using the Berry-phase approach proposed by R. D. King-Smith and D. Vanderbilt[25,26], we have calculated the spontaneous electric polarization of LN-type $ZnTiO_3$ based on finite electric field calculations. The results show that the polarizations of P_x and P_y are almost equal to zero, so the polarization lies mainly along the z-axis direction. The total polarization is composed of the ionic (P_{ion}) and electronic (P_{ele}) contributions. The results based on LDA show that the total polarization is 90.43 μC/cm², and the values of P_{ion} and P_{ele} are 89.07 μC/cm² and 1.36 μC/cm², respectively. Therefore, the electric polarization mainly arises from the ionic contribution. Based on the result of our GGA calculation, the total polarization is 93.14 μC/cm², the vales of P_{ion} and electronic P_{ele} are 91.73 μC/cm² and 1.41 μC/cm². According to ref. [14], the values of polarization obtained by Born effective charges and nominal charge are 88 μC/cm² and 75 μC/cm². Our results are slightly larger than their values and consistent with their results based on Born effective charges.

The Born effective charges of the LN-type $ZnTiO_3$ are presented in Table 2. The nominal charges of Zn, Ti and O are +2, +4 and −2, respectively. By comparing the Born effective charges of these ions and their nominal values, it is found that charge numbers Z^* of Zn, Ti and O (especially for Z_{xx}^* and Z_{yy}^* in Ti atom, Z_{yy}^* in O1, and Z_{xx}^* in O2 atoms) are obvious anomalous, which is an important characteristic in ferroelectric materials. From Table 2, one can see that Z^* of Zn and Ti atoms mainly occur on the diagonal elements, and the values of the non-diagonal elements are small or equal to zero. This is in consistent with the spontaneous polarization being mainly along the z-axis direction. Compared with Z^* of Zn and Ti atoms, the Z^* tensor of O atoms displays strong anisotropy, and this should be attributed to the structural distortions caused by the Zn 3d-O 2p and Ti 3d-O 2p orbital hybridizations.

Zone-center phonon modes. In ferroelectric crystals that have undergone the paraelectric to ferroelectric transition, the relative displacements of anions and cations will lower the symmetry and lead to spontaneous polarization. This phenomenon can be explained by the theory of soft zone-center phonon modes. Firstly, we perform the symmetry analyses in $ZnTiO_3$ and divide its zone-center phonon modes into irreducible representations. The two paraelectric phases of $ZnTiO_3$ are ilmenite (IL)-type (hexagonal space group $R\bar{3}$) and Perovskite (Pv)-type (orthorhombic space group Pnma) structures, and the ferroelectric phase is $LiNbO_3$-type structure (hexagonal space group R3c). In this compound, there exists a continuous phase transition from ilmenite-type structure to perovskite-type, and then to $LiNbO_3$-type structure.

In high-symmetry IL-type $ZnTiO_3$ (space group $R\bar{3}$), there are 10 atoms in the primitive cell. All the 30 modes (including 3 acoustic modes) are composed of 4 irreducible representations (irreps).

$$\Gamma(R\bar{3}) = 5A_g \oplus 10E_g^* \oplus 5A_u \oplus 10E_u^* \tag{5}$$

In these modes, the three acoustic modes are composed of one A_u and two E_u^* modes. In the optical modes, A_g and E_g^* are Raman active, while A_u and E_u are infrared (IR) active. The corresponding zone-center optical phonon modes are presented in Table 3. In its perovskite-type paraelectric phase (space group Pnma), there are 20 atoms in the primitive cell. All the 60 phonon modes at Γ point (including three acoustic modes) are composed of 8 irreps.

$$\Gamma(\mathrm{Pnma}) = 7A_g \oplus 5B_{1g} \oplus 7B_{2g} \oplus 5B_{3g} \oplus 8A_u \oplus 10B_{1u} \oplus 8B_{2u} \oplus 10B_{3u} \tag{6}$$

Among them, three acoustic modes are in B_{1u}, B_{2u} and B_{3u}, respectively. The optical modes of A_g, B_{1g}, B_{2g} and B_{2g} are Raman active; the optical modes of B_{1u}, B_{1u} and B_{3u} are IR active, while the A_u modes are silent. We present

A_u	A_g	E_u	E_g
182.88	137.31	187.49	172.99
368.25	213.20	267.39	248.74
469.14	356.79	387.31	309.73
660.88	442.07	481.90	453.06
	678.17		578.94

Table 3. The calculated frequency (cm^{-1}) of zone-center optical phonon modes of ilmenite (IL)-type $ZnTiO_3$ (space group $R\bar{3}$).

A_g	A_u	B_{1g}	B_{2g}	B_{3g}	B_{1u}	B_{2u}	B_{3u}
105.09	74.20	173.82	137.82	131.12	63.56	124.12i	101.57i
153.48	102.07	244.52	163.07	304.52	111.09	74.88	95.45
241.88	113.28	356.88	250.55	454.52	183.91	127.15	178.83
300.53	151.47	467.27	370.45	462.60	305.34	219.98	223.22
434.00	283.65	654.80	467.71	747.05	332.94	397.35	325.38
451.84	379.67		509.34		370.06	413.30	366.11
509.22	394.47		729.64		440.83	472.24	430.89
	490.47				461.78		489.77
					516.84		547.12

Table 4. The frequencies (cm^{-1}) of zone-center optical phonon modes in the perovskite (Pv)-type $ZnTiO_3$.

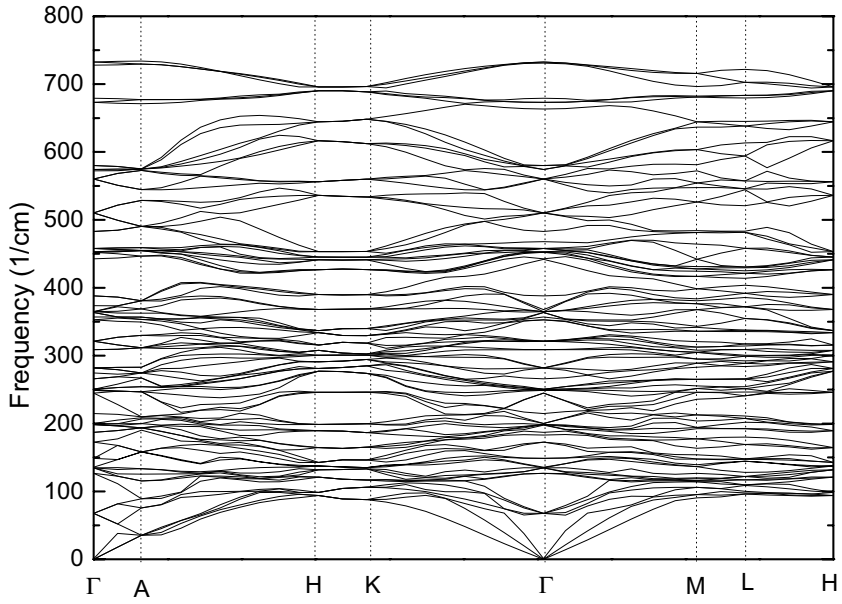

Figure 6. The phonon dispersion relations of the ilmenite (IL)-type $ZnTiO_3$ (space group $R\bar{3}$) along high symmetry directions based on GGA.

the corresponding zone-center optical phonon modes in Table 4. From this table, it is found that there are two imaginary frequencies in B_{2u} (124.12i) and B_{3u} (101.57i), respectively. However, in its high-symmetry IL-type $ZnTiO_3$, according to Table 3, it is found that there are no imaginary frequencies in the zone-center phonon optical modes; additionally, we also calculated its phonon dispersion spectrum, and it is found that there are no imaginary frequencies in these phonon modes. In order to verify the stability of the R3c and R-3 structures, we also carried out the phonon dispersion relationship based on GGA. Figures 6 and 7 present the phonon dispersion relations of the IL-type (space group $R\bar{3}$) and LN-type $ZnTiO_3$ (space group R3c) along high symmetry directions. According to these two figures, it can be clearly seen that phonon frequencies of the two structures at the Γ point are both zero. The calculated total energies based on norm-conserving pseudopotentials in its paraelectric (IL-type $R\bar{3}$ and Pv-type pnma) and ferroelectric phases (LN-type R3c) are −8308.8749 ($R\bar{3}$), −8308.37359 (pnma) and −8308.5650 (R3c) eV within LDA; and −8321.4057 ($R\bar{3}$), −8320.7809 (pnma) and

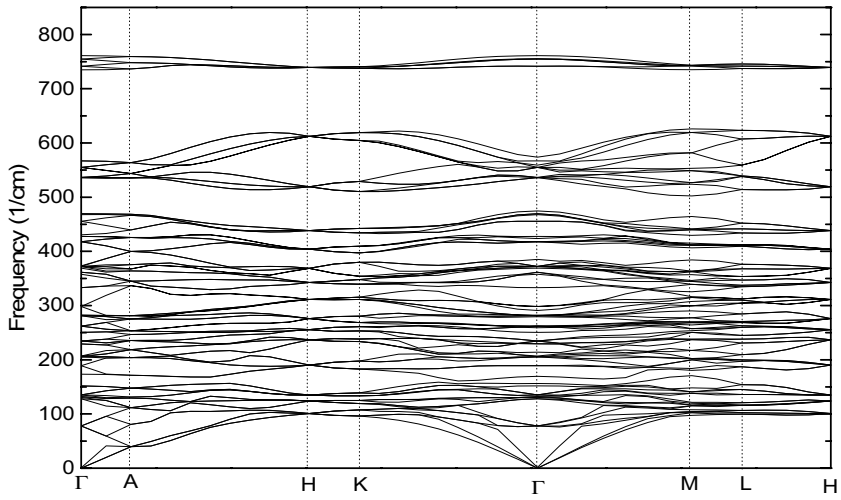

Figure 7. The phonon dispersion relations of the LN-type $ZnTiO_3$ (space group R3c) along high symmetry directions based on GGA.

A_1 (TO)	A_1 (LO)	E (TO)	E (LO)	A2
142.56	165.26	141.16	152.71	120.69
281.53	325.70	194.64	204.87	363.21
387.55	436.30	223.63	223.88	417.04
653.83	826.10	265.30	267.41	468.54
		321.53	325.71	839.51
		343.16	428.20	
		436.96	479.11	
		639.91	656.14	
		657.30	848.01	

Table 5. The frequencies (cm^{-1}) of transverse optical (TO) and longitudinal optical (LO) zone-center optical phonon modes of the $LiNbO_3$-type $ZnTiO_3$.

−8321.0790 (R3c) eV within GGA. The results show that the energy of its IL-type paraelectric phase is the lowest, the energy of Pv-type paraelectric phase is the highest, and the energy of LN-type ferroelectric phase lies in the middle. In order to verify whether it is due to the inaccuracy of the exchange correlation, we have carried out total energy calculation based on PBEsol, which is intended to improve on PBE for equilibrium properties such as bond lengths and lattice parameters. The calculated lattice parameters of PBEsol are also presented in Table 1. The results show that total energies are −8302.8974 ($R\bar{3}$), −8302.3911 (pnma) and −8302.5810 (R3c) eV based on PBEsol. This is consistent with the above conclusion $E(R\bar{3}) < E(R3c) < E(pnma)$. This should be attributed to the synthesis of LN-type ZnTiO3 under high pressure.

In the ferroelectric phase (space group R3c) in $ZnTiO_3$, the primitive cell contains 10 atoms, so there are 30 phonon modes at the Γ point. The three zero-frequency acoustic modes comprise one in A_1 and two in E. The zone-center phonon optical modes are as follows:

$$\Gamma(R3c) = 4A_1 \oplus 5A_2 \oplus 9E \tag{7}$$

In these modes, A_1 and E optical modes are both Raman and infrared (IR) active, while A_2 modes are silent. The optical modes of the LN-type $ZnTiO_3$ (see in Table 5) infer that the imaginary frequencies disappear from perovskite-type paraelectric phase to $LiNO_3$-type ferroelectric phase. Due to A1 and E optical modes being IR active, these frequencies are splitting into LO and TO modes described by the Lyddane–Sachs–Teller (LST) relation[50]. Generally, the large Bern effective charge corresponds to a large LO-TO splitting. From Table 5, one can see that three A_1 modes (281.53~325.70 cm^{-1}, 387.55 ~436.30 cm^{-1}, and 653.93~826.10 cm^{-1}) and three E modes (343.16~428.20 cm^{-1}, 436.96~479.11 cm^{-1}, and 657.30~848.01 cm^{-1}) show large LO-TO splitting. In Table 6, we present the mode effective charges and mode-oscillator strengths corresponding to the zone-center transverse optical (TO) modes of LN-type $ZnTiO_3$.

Piezoelectric properties. In order to investigate the structural stability and piezoelectric properties of LN-type $ZnTiO_3$, we calculate the elastic and piezoelectric constants by treating homogeneous strains as perturbations based on DFPT. According to the calculated results, the six independent elastic coefficients (Voigt notations) of this compound are C_{11}, C_{12}, C_{13}, C_{14}, C_{33}, and C_{44}, respectively. Additionally, it should be pointed out

A_1 modes ($ZnTiO_3$)			E modes ($ZnTiO_3$)		
ω	Z_m^*	S_m	ω	Z_m^*	S_m
142.56	3.61	1.97	141.16	2.47	1.09
281.53	6.51	10.05	194.64	2.50	1.01
387.55	0.50	0.08	223.63	0.30	0.02
653.83	5.63	10.35	265.30	1.18	0.40
			321.53	3.68	2.54
			343.16	6.02	10.07
			436.96	1.33	0.59
			639.91	6.15	12.06
			657.30	1.73	0.84

Table 6. The calculated mode effective charges (|e|), and mode-oscillator strengths (within 10^{-4} atomic units) corresponding to the zone-center transverse optical phonon modes of $LiNbO_3$-type $ZnTiO_3$.

Elastic stiffness coefficients C_{ij} ($10^{11}N/m^2$)							
material	C_{11}	C_{12}	C_{13}	C_{15}	C_{33}	C_{44}	C_{66}
$ZnTiO_3$	3.675	1.875	1.442	0.031	2.877	0.800	0.899
$ZnSnO_3$ ref. [43]	1.94	0.63	1.01	0.001	1.69	1.17	0.92
	C_{11}	C_{12}	C_{13}	C_{14}	C_{33}	C_{44}	C_{66}
$LiNbO_3$ ref. [44]	2.03	0.53	0.75	0.09	2.45	0.60	0.75
$LiTaO_3$ ref. [44]	2.298	0.440	0.812	−0.104	2.798	0.968	0.929

Table 7. The Elastic stiffness coefficients of LN-type $ZnTiO_3$.

Piezoelectric stress constants e_{ij} (C/m^2)				
Material	e_{11}	e_{15}	e_{31}	e_{33}
$ZnTiO_3$	−0.93	1.00	1.01	2.51
$PbTiO_3$ ref. [54 a]		6.63	2.06	4.41
$PbTiO_3$ ref. [54 b]		6.66	2.07	4.48
$ZnSnO_3$ ref. [43]	−0.15	0.26	1.23	0.29
$ZnGeO_3$ ref. [43]	−0.27	0.36	0.65	2.81
	e_{22}	e_{15}	e_{31}	e_{33}
$LiNbO_3$ ref. [44]	2.43	3.76	0.23	1.33
$LiTaO_3$ ref. [44]	1.67	2.72	−0.38	1.09

Table 8. The piezoelectric stress constants (relaxed ion) of LN-type $ZnTiO_3$, it is noted that a and b in $PbTiO_3$ represents DFPT finite strain method, respectively.

that $C_{66} = (C_{11} - C_{12})/2$. In Table 7, we give the corresponding elastic stiffness coefficients (relaxed ion) of LN-type $ZnTiO_3$. The point group of LN-type $ZnTiO_3$ belongs to the triangle crystal. As discussed in refs. [51,52], the triangle crystals need to satisfy the following Born mechanical stability criterion.

$$\begin{aligned} &C_{11} - |C_{12}| > 0 \\ &(C_{11} + C_{12})C_{33} - 2C_{13}^2 > 0 \\ &(C_{11} - C_{12})C_{44} - 2C_{15}^2 > 0 \end{aligned} \tag{8}$$

The results presented in Table 7 reveal that the elastic constants of the LN-type $ZnTiO_3$ satisfy the constraints of the Born stability condition. Therefore, the structure of LN-type $ZnTiO_3$ is stable. By using homogeneous strains and electric fields as perturbations, we can calculate the piezoelectric properties of LN-type $ZnTiO_3$. The obtained piezoelectric tensor of this compound has the four independent elements (Voigt notations) e_{11}, e_{15}, e_{31}, e_{33}:

$$e = \begin{pmatrix} e_{11} & -e_{11} & 0 & 0 & e_{15} & 0 \\ 0 & 0 & 0 & e_{15} & 0 & 0 \\ e_{31} & e_{31} & e_{33} & 0 & 0 & 0 \end{pmatrix} \tag{9}$$

Obviously, this tensor is the same as that of LN-type $ZnSnO_3$ and $ZnGeO_3$, however it is a little different from that of $LiNbO_3$ and $LiTaO_3$ since independent elements of the piezoelectric tensor in $LiNbO_3$ and $LiTaO_3$ are e_{22}, e_{15}, e_{31}, and e_{33}. In Table 8, we present the piezoelectric constants of LN-type $ZnTiO_3$, $ZnSnO_3$ and $ZnGeO_3$

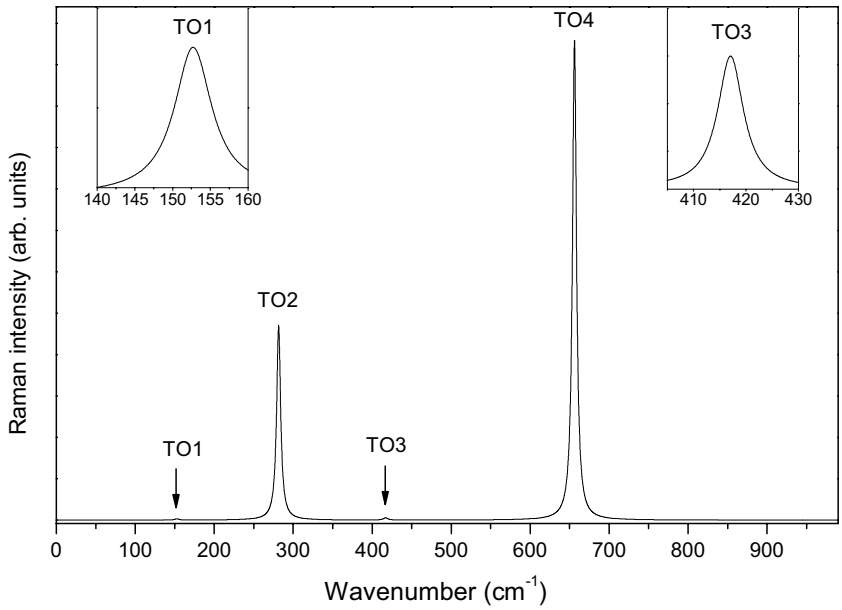

Figure 8. The calculated Raman spectra of $LiNbO_3$-type $ZnTiO_3$ for a x(zz)y scattering configuration in the range of 0~1000 cm^{-1}. The spectra displays the TO of A_1 modes.

together with $LiNbO_3$ and $LiTaO_3$[30,53]. From this table, the piezoelectric constants e_{11}, e_{15}, e_{31}, e_{33} are −0.93, 1.00, 1.01 and 2.51 C/m^2, respectively. It is well known that lead titanate ($PbTiO_3$) piezoelectric ceramics have excellent piezoelectric properties[54,55]. By comparing the piezoelectric coefficients of LN-type ZnTiO and that of $PbTiO_3$[55] calculated by density functional pertubation theory and finite strain method (see Table 8), it is found that values of e_{31}, e_{33} of LN-type $ZnTiO_3$ are close to and exceeds one-half of that of $PbTiO_3$, and the value of e_{15} is relatively small compared to that of $PbTiO_3$. The large piezoelectric constants reveal that LN-type $ZnTiO_3$ is a promising candidate piezoelectric material.

Nonlinear optical properties. As mentioned above, the zone-center phonon optical modes of ferroelectric phase $ZnTiO_3$ can be divided into $4A_1 \oplus 5A_2 \oplus 9E$, and A_1 and E modes are both Raman and infrared active. The Raman scattering efficiencies of the phonon modes can be calculated using the following formula[56,57]:

$$\frac{dS}{d\Omega} = \frac{(\omega_0 - \omega_m)^4}{c^4} |e_s \cdot \alpha_m \cdot e_0|^2 \frac{\hbar}{2\omega_m}(n_m + 1) \tag{10}$$

where α_m, c, $\hbar$ and n_m are the Raman susceptibility, the speed of light in vacuum, the Planck constant and Bose-Einstein factor, respectively; ω_0 and ω_m are the frequencies of an incoming photon and the mth zone-center phonon mode, the frequency of scattered outgoing photon is $(\omega_0 - \omega_m)$, e_s and e_0 indicate incoming and outgoing polarizations within an angle Ω. According to the structural symmetry, the Raman tensors of A_1 mode (along z axis) and E mode (in the x-y plane) of LN-type $ZnTiO_3$ are similar to that of $LiNbO_3$ and described as follows:

$$A_1(z) = \begin{pmatrix} a & 0 & 0 \\ 0 & a & 0 \\ 0 & 0 & b \end{pmatrix} \tag{11}$$

$$E(x) = \begin{pmatrix} c & 0 & d \\ 0 & -c & 0 \\ d & 0 & 0 \end{pmatrix} \quad E(y) = \begin{pmatrix} 0 & c & 0 \\ c & 0 & -d \\ 0 & -d & 0 \end{pmatrix} \tag{12}$$

Figure 8 displays the calculated Raman spectrum of $LiNbO_3$-type $ZnTiO_3$ for the x(zz)y scattering configuration. In this configuration, as in the case of $LiNbO_3$ or $PbTiO_3$, only the transverse A_1 modes can be detected. In order to see the peaks of TO1 and TO3 clearly, we have made two enlarged small illustrations in this figure. The results show that TO2 and TO4 modes have a very strong Raman scattering efficiency. In comparison, the Raman scattering efficiencies of TO1 and TO3 are very weak and are much smaller than that of the TO2 and TO4 modes. As presented in Tables 5 and Table 6, notice that TO2 and TO4 of A_1 modes have large LO-TO splittings and oscillator strengths, and the two frequencies just correspond to large Raman peaks. Figure 9 presents the calculated Raman spectrum of $LiNbO_3$-type $ZnTiO_3$ for the x(yz)y configuration. In this configuration, the same as $LiNbO_3$, only the TO and LO of E modes can be detected. From this figure, it is found that five transverse modes (TO3, TO4, TO6 and TO7 and TO8) and five longitudinal modes (LO2, LO3, LO4, LO7 and LO9) have strong Raman scattering efficiency. Due to the LO-TO splittings of LO3(223.63 cm^{-1})-TO3(223.88 cm^{-1}) and LO4(265.30 cm^{-1})-TO4(267.41 cm^{-1}) being very small, the two Raman intensity peaks almost completely overlap.

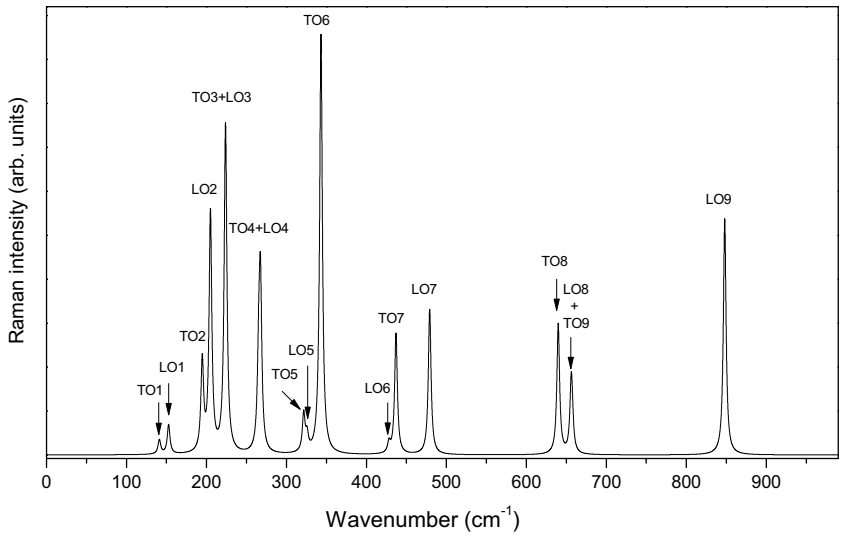

Figure 9. The calculated Raman spectra of the $LiNbO_3$-type $ZnTiO_3$ for a x(yz)y scattering configuration of E modes in the range of 0~1000 cm^{-1}.

Nonlinear optical susceptibilities d_{ij} (Pm/V)			
	d_{12}	d_{31}	d_{33}
$ZnTiO_3$	1.37	1.46	−20.18
$ZnSnO_3$ ref. [31]	13.09	1.73	11.06
$ZnGeO_3$ ref. [30]	3.14	6.16	8.45
	d_{22}	d_{31}	d_{33}
$LiNbO_3$ ref. [56]	−6.25	3.60	−37.5
$LiTaO_3$ ref. [57]	−1.07	−1.07	−16.40

Table 9. The calculated nonlinear optical susceptibilities of LN-type $ZnTiO_3$.

The LN-type $ZnTiO_3$ belongs to the 3 m point group, therefore this compound is a candidate promising nonlinear optical material. As discussed by Inaguma *et al.*[14], the SHG response of LN-type $ZnTiO_3$ is 24 times greater than that of LN-type $ZnSnO_3$ and has about 5% of the SHG response of $LiNbO_3$. By using electric fields and atomic displacements as perturbations based on DFPT, we have calculated the nonlinear optical (NLO) susceptibilities and electro-optic (EO) coefficients of LN-type $ZnTiO_3$. According to reports by M. Veithen, *et al.*[48], the NLO properties of various semiconductors, such as $LiNbO_3$, PbTiO3, and AlAs, etc. were calculated by DFPT based on the ABINIT package. The comparation between the theoretical results of NLO and EO coefficients with the experimental data shows that the method is reliable. The calculated results show that the three independent elements of the NLO tensor of this compound are d_{12}, d_{15} and d_{33} (Voigt notations).

$$d = \begin{pmatrix} -d_{12} & d_{12} & 0 & 0 & d_{15} & 0 \\ 0 & 0 & 0 & d_{15} & 0 & d_{12} \\ d_{15} & d_{15} & d_{33} & 0 & 0 & 0 \end{pmatrix} \tag{13}$$

The NLO tensor form of LN-type $ZnTiO_3$ is the same as that of LN-type $ZnSnO_3$ and $ZnGeO_3$, but it is not the same as that of $LiNbO_3$ and $LiTaO_3$ since the independent elements of NLO tensor of the latter are d_{22}, d_{31}, d_{33}. The calculated NLO susceptibilities of LN-type $ZnTiO_3$ together with those of LN-type $ZnGeO_3$[43], LN-type $ZnSnO_3$[31], $LiNbO_3$[58] and $LiTaO_3$[59] are presented in Table 9. From this table, the NLO susceptibilities d_{12}, d_{15} and d_{33} are 1.37, 1.46 and −20.18 Pm/V, respectively, and one can see that the biggest susceptibility (d_{33}) of this compound is larger than that of $ZnSnO_3$, and lower than that of $LiNbO_3$. For the electro-optic (EO) coefficients of LN-type $ZnTiO_3$, the results reveal that its independent elements are γ_{11}, γ_{13}, γ_{33}, and γ_{51}.

$$\gamma = \begin{pmatrix} \gamma_{11} & 0 & \gamma_{13} \\ -\gamma_{11} & 0 & \gamma_{13} \\ 0 & 0 & \gamma_{33} \\ 0 & \gamma_{51} & 0 \\ \gamma_{51} & 0 & 0 \\ 0 & -\gamma_{11} & 0 \end{pmatrix} \tag{14}$$

Electro-optic tensors γ_{ij} (Pm/V)				
	γ_{11}	γ_{13}	γ_{33}	γ_{51}
$ZnTiO_3$	0.46	3.71	17.17	1.62
$ZnSnO_3$ ref. [30]	1.23	1.57	−2.78	0.54
$ZnGeO_3$ ref. [31]	0.44	1.68	5.56	0.85
	γ_{22}	γ_{31}	γ_{33}	γ_{33}
$LiNbO_3$ ref. [58]	8.6	30.8	3.4	28
$LiTaO_3$ ref. [59]	35	8.2	20	0.5

Table 10. The calculated Electro-optic tensor of LN-type $ZnTiO_3$.

As can be seen, the EO tensor is the same as that of LN-type $ZnSnO_3$ and $ZnGeO_3$, but is different from that of $LiNbO_3$ and $LiTaO_3$ since the independent elements of latter are γ_{13}, γ_{33}, γ_{22} and γ_{51}. The EO coefficients can be divided into three contributing parts: electronic, ionic and piezoelectric. In Table 10, we give the calculated EO coefficients of LN-type $ZnTiO_3$. For ease of comparison, the EO coefficients of LN-type $ZnGeO_3$, LN-type $ZnSnO_3$, $LiNbO_3$[60] and $LiTaO_3$[61] are also listed in this table. Our obtained EO coefficients γ_{11}, γ_{13}, γ_{33}, and γ_{51} for LN-type $ZnTiO_3$ are 0.46, 3.71, 17.17 and 1.62 Pm/V, respectively. Obviously, the coefficients γ_{13} and γ_{33} are much larger than that of LN-type $ZnSnO_3$ and $ZnGeO_3$. The large NLO susceptibilities and EO coefficients reveal that the LN-type $ZnTiO_3$ is a high performance lead-free nonlinear optical crystal.

Conclusions

In this work, the electronic structure, zone-center phonon modes, piezoelectric and nonlinear optical properties of LN-type $ZnTiO_3$ are investigated by first-principles calculations based on DFT. The electronic structure shows that this compound is a wide direct-band-gap insulator. By investigating the zone-center phonon modes of the paraelectric and ferroelectric phases, it is found that there are two imaginary frequencies in B_{2u} and B_{3u} in the perovskite paraelectric phase, and subsequently the imaginary frequencies disappear in the ferroelectric phase. The calculated spontaneous polarizations are 90.43 $\mu C/cm^2$ and 93.14 $\mu C/cm^2$ based on LDA and GGA, respectively. Our results are in good agreement with the experimental results, and the large spontaneous polarization reveals that this compound is a good ferroelectric material.

The elastic constants of LN-type $ZnTiO_3$ satisfy the constraints of the Born stability condition, and therefore this compound has a stable structure. The obtained piezoelectric tensor has four independent elements e_{11}, e_{15}, e_{31}, e_{33}, with values −0.93, 1.00, 1.01 and 2.51 C/m^2. This shows that this compound is a promising piezoelectric crystal. Like $LiNbO_3$, the calculated Raman spectrum for the x(zz)y and x(yz)y configurations correspond to A_1 and E modes, and the Raman scattering peaks of A_1 and E modes are assigned to their zone-center optical modes, respectively. The independent nonlinear optical susceptibilities of this compound are d_{12}, d_{15} and d_{33} with values 1.37, 1.46 and −20.18 Pm/V, respectively. For the EO coefficients, the independent elements are γ_{11}, γ_{13}, γ_{33}, and γ_{51} with values 0.46, 3.71, 17.17 and 1.62 Pm/V, respectively. The results show that LN-type $ZnTiO_3$ exhibits better nonlinear optical properties than LN-type $ZnSnO_3$. The large piezoelectric and nonlinear optical susceptibilities reveal that this compound is a high-performance lead-free piezoelectric and nonlinear optical crystal.

Received: 21 June 2019; Accepted: 29 October 2019;
Published online: 26 November 2019

References

1. Halasyamani, P. S. & Poeppelmeier, K. R. Noncentrosymmetric Oxides. *Chemistry of Materials* **10**, 2753–2769 (1998).
2. Cammarata, A., Zhang, W., Halasyamani, P. S. & Rondinelli, J. M. Microscopic Origins of Optical Second Harmonic Generation in Noncentrosymmetric-Nonpolar Materials. *Chemistry of Materials* **26**, 5773–5781 (2014).
3. Wu, C., Yang, G., Humphrey, M. G. & Zhang, C. Recent advances in ultraviolet and deep-ultraviolet second-order nonlinear optical crystals. *Coordination Chemistry Reviews* **375**, 459–488 (2018).
4. Tran, T. T., Halasyamani, P. S. & Rondinelli, J. M. Role of Acentric Displacements on the Crystal Structure and Second-Harmonic Generating Properties of $RbPbCO_3F$ and $CsPbCO_3F$. *Inorganic chemistry* **53**, 6241–6251 (2014).
5. Shearer, M. J. *et al*. Complex and Noncentrosymmetric Stacking of Layered Metal Dichalcogenide Materials Created by Screw Dislocations. *J. Am. Chem. Soc* **139**, 3496–3504 (2017).
6. Nguyen, S. D., Yeon, J., Kim, S. H. & Halasyamani, P. S. $BiO(IO_3)$: A new polar iodate that exhibits an Aurivillius-type $(Bi2O_2)^{2+}$ layer and a large SHG response. *J Am Chem Soc* **133**, 12422–12425 (2011).
7. Halasyaman, P. S. Asymmetric Cation Coordination in Oxide Materials: Influence of Lone-Pair Cations on the Intra-octahedral Distortion in d0 Transition Metals. *Chem. Mater.* **16**, 3586–3592 (2004).
8. Inaguma, Y. *et al*. Synthesis, Structural Transformation, Thermal Stability, Valence State, and Magnetic and Electronic Properties of $PbNiO_3$ with Perovskite- and $LiNbO_3$-Type Structures. *J Am Chem Soc* **133**, 16920–16929 (2011).
9. Yu, R., Hojo, H., Mizoguchi, T. & Azuma, M. Giant dielectric response and low dielectric loss in Al_2O_3 grafted $CaCu_3Ti_4O_{12}$ ceramics. *J. Appl. Phys.* **118**, 094103 (2015).
10. Coomer, F. C., Checker, N. J. & Wright, A. J. Jahn-Teller Distorted Frameworks and Magnetic Order in the Rb-Mn-P-O System. *Inorg. Chem.* **49**, 934–942 (2010).
11. Li, M. *et al*. $Ba_3(Cr_{0.97(1)}Te_{0.03(1)})_2TeO_9$: in Search of Jahn–Teller Distorted Cr(II) Oxide. *Inorg. Chem*, **55**, 10135–10142 (2016).
12. Fan, Y. H. *et al*. $Ba_3(Cr_{0.97(1)}Te_{0.03(1)})_2TeO_9$: in Search of Jahn–Teller Distorted Cr(II) Oxide. *Inorg. Chem* **56**, 114–124 (2017).
13. Navrotsky, A. Energetics and Crystal Chemical Systematics among Ilmenite, Lithium Niobate, and Perovskite Structures. *Chem. Mater.* **10**, 2787 (1998).
14. Inaguma, Y. *et al*. High-pressure synthesis, crystal structure, and phase stability relations of a $LiNbO_3$-type polar titanate $ZnTiO_3$ and its reinforced polarity by the second-order Jahn-Teller effect. *J. Am. Chem. Soc.* **136**, 2748–2756 (2014).

15. Bartram, S. F. & Slepetys, A. Compound Formation and Crystal Structure in the system ZnO-TiO_2. *J. Am. Ceram. Soc.* **44**, 493 (1961).
16. Ito, E. & Matsui, Y. High-Pressure Transformations in Silicates, Germanates, and Titanates With ABO_3 Stoichiometry. *Phys. Chem. Miner.* **4**, 265 (1979).
17. Linton, J. A., Fei, Y. & Navrotsky, A. Complete Fe-Mg solid solution in lithium niobate and perovskite structures in titanates at high pressures and temperatures. *Am. Mineral.* **82**, 639 (1997).
18. Inaguma, M., Yoshiyuki, Y. & Katsumata, T. A Polar Oxide $ZnSnO_3$ with a $LiNbO_3$-Type Structure. *J. Am. Chem. Soc* **130**, 6704–6705 (2008).
19. Varga, T. *et al*. Coexistence of weak ferromagnetism and ferroelectricity in the high pressure $LiNbO_3$-type phase of $FeTiO_3$. *Phys.rev. lett.* **103**, 047601 (2009).
20. Leinenweber, K. *et al*. High-pressure perovskites on the join $CaTiO_3$-$FeTiO_3$. *Phys. Chem. Miner.* **21**, 207 (1994).
21. Leinenweber, K. High-pressure synthesis and study of low-compressibility molybdenum nitride (MoN and MoN_{1-x}) phases. *Phys. Chem. Miner.* **22**, 251 (1995).
22. Hattori, T. *et al*. Clinopyroxene-perovskite phase transition of $FeGeO_3$ under high pressure and room temperature. *Phys. Chem. Miner.* **26**, 212 (1999).
23. Yusa, H. *et al*. High-pressure transformations of ilmenite to perovskite, and lithium niobate to perovskite in zinc germanate. *Physics and Chemistry of Minerals.* **33**, 217–226 (2006).
24. Deng, X., Lu, W., Wang, H., Huang, H. & Dai, J. Electronic, magnetic and dielectric properties of multiferroic $MnTiO_3$. *Journal of Materials Research*. **27**, 1421–1429 (2012).
25. King-Smith, R. D. & Vanderbilt, D. Theory of polarization of crystalline solids. *Phys. Rev. B.* **47**, 1651–1654 (1993).
26. Vanderbilt, D. & King-Smith, R. D. Electric polarization as a bulk quantity and its relation to surface charge. *Phys. Rev. B* **48**, 4442–4455 (1993).
27. Baroni, S., Gironcoli, S. & Corso, A. D. Phonons and related crystal properties from density-functional perturbation theory. *Rev. Mod. Phys.* **73**, 515 (2001).
28. Shaltaf, R., Durgun, E., Raty, J. Y., Ghosez, P. & Gonze, X. Dynamical, dielectric, and elastic properties of GeTe investigated with first-principles density functional theory. *Phys. Rev. B.* **78**, 205203 (2008).
29. Shaltaf, R., Gonze, X., Cardona, M., Kremer, R. K. & Siegle, G. Lattice dynamics and specific heat of α-GeTe: Theoretical and experimental study. *Phys. Rev. B.* **79**, 075204 (2009).
30. Zhang, J. *et al*. First-principles study of the ferroelectric and nonlinear optical properties of the $LiNbO_3$-type $ZnSnO_3$. *Phys. Chem. Chem. Phys.* **12**, 9197–9204 (2010).
31. Zhang, J., Xu, B., Qin, Z., Li, X. F. & Yao, K. L. Ferroelectric and nonlinear optical properties of the $LiNbO_3$-type $ZnGeO_3$ from first-principles study. *Journal of Alloys and Compounds.* **514**, 113 (2012).
32. Lu, X. Z., Whangbo, M.-H., Dong, S., Gong, X. G. & Xiang, H. J. Giant Ferroelectric Polarization of $CaMn_7O_{12}$ Induced by a Combined Effect of Dzyaloshinskii-Moriya Interaction and Exchange Striction. *Phys. Rev. Lett.* **108**, 187204 (2012).
33. Yang, J. H. *et al*. Strong Dzyaloshinskii-Moriya Interaction and Origin of Ferroelectricity in Cu_2OSeO_3. *Phys. Rev. Lett.* **109**, 107203 (2012).
34. Ding, W. *et al*. Prediction of intrinsic two-dimensional ferroelectrics in In_2Se_3 and other III_2-VI_3 van der Waals materials. *Nature Communications.* **8**, 14956 (2017).
35. Liu, H. M. *et al*. Metallic ferroelectricity induced by anisotropic unscreened Coulomb interaction in $LiOsO_3$. *Physical Review B.* **91**, 064104 (2015).
36. Filippetti, A. *et al*. Prediction of a native ferroelectric metal. *Nature Communications* **7**, 1121 (2016).
37. Gonze, X. *et al*. Capabilities and prospects: Zeitschrift für *Kristallog*raphie- Crystalline Materials. *Z. Kristallogr.* **200**, 558 (2005).
38. Gonze, X. *et al*. ABINIT: First-Principles Approach of Materials and Nanosystem Properties. *Comput. Phys. Commun.* **180**, 2582 (2009).
39. Vanderbilt, D. Soft self-consistent pseudopotentials in a generalized eigenvalue formalism. *Phys. Rev. B.* **41**, 7892 (1990).
40. Kresse, G. & Hafner, J. Ab initio molecular dynamics for liquid metals. *Phys. Rev. B.* **47**, RC558 (1993).
41. Kresse, G. & Furthmuller, J. Efficient iterative schemes for ab initio total-energy calculations using a plane-wave basis set. *Phys. Rev. B* **54**, 11169 (1996).
42. Lu, Z. S. *et al*. Phosphorene: A promising metal free cathode material for proton exchange membrane fuel cell. *Applied Surface Science* **479**, 590 (2019).
43. Monkhorst, H. J. & Pack, J. D. Special points for Brillouin-zone integrations. *Phys. Rev. B.* **13**, 5188 (1976).
44. Perdew, J. P., Burke, K. & Ernzerhof, M. Generalized Gradient Approximation Made Simple. *Phys. Rev. Lett.* **77**, 3865 (1996).
45. Heyd, J., Scuseria, G. E. & Ernzerhof, M. Hybrid Functionals Based on a Screened Coulomb Potential. *J. Chem. Phys.* **118**, 8207–8215 (2003).
46. Krukau, A. V., Vydrov, O. A., Izmaylov, A. F. & Scuseria, G. E. Influence of the exchange screening parameter on the performance of screened hybrid functionals. *J. Chem. Phys.* **125**, 224106 (2006).
47. Nunes, R. W. & Vanderbilt, D. Theory of Polarization: A Modern Approach. *Phys. Rev. Lett.* **73**, 712 (1994).
48. Veithen, M., Gonze, X. & Ghosez, P. Nonlinear optical susceptibilities, Raman efficiencies, and elctro-optic tensors from first-principles density functional perturbation theory. *Phys. Rev. B.* **71**, 125107 (2005).
49. Wemple, S. H. & DiDomomenico, D. Jr. In *Applied Solid State Science*, edited by Wolfe, R. (Academic, New York, 1972).
50. Lyddane, R., Sachs, R. & Teller, E. On the Polar Vibrations of Alkali Halides. *Physical Review.* **59**, 673–676 (1941).
51. Tse, J. S. & Klug, D. D. Mechanical instability of alpha-quartz: A molecular dynamics study. *Phys. Rev. Lett.* **67**, 3559 (1991).
52. Tse, J. S. & Klug, D. D. Anisotropy in the structure of pressure-induced disordered solids. *Phys. Rev. Lett.* **70**, 174 (1993).
53. Smith, R. T. & Welsh, F. S. Temperature Dependence of the Elastic, Piezoelectric, and Dielectric Constants of Lithium Tantalate and Lithium Niobate. *J. Appl. Phys.* **42**, 2219 (1971).
54. Cazorla, C. Electrostatic engineering of strained ferroelectric perovskites from first-principles. *Phys. Rev. B* **92**, 214108 (2015).
55. Wu, Z. & Cohen, R. E. Pressure-Induced Anomalous Phase Transitions and Colossal Enhancement of Piezoelectricity in $PbTiO_3$. *Phys. Rev. Lett.* **95**, 037601 (2005).
56. Troeye, B. V., Gillet, Y., Poncé, S. & Gonze, X. First-principles characterization of the electronic and optical properties of hexagonal $LiIO_3$. *Optical Materials.* **36**, 1494–1501 (2014).
57. Hermet, P., Veithen, M. & Ghosez, P. First-principles calculations of the nonlinear optical susceptibilities and Raman scattering spectra of lithium niobate. *J. Phys:Condens Matter.* **19**, 456202 (2007).
58. Johnston, W. D. Jr. Nonlinear Optical Coefficients and the Raman Scattering Efficiency of LO and TO Phonons in Acentric Insulating Crystals. *Phys. Rev. B.* **1**, 3494 (1970).
59. Weber. M. J. (Editor-in-Chief) 2003 *Handbook of Optical Materials*. (Boca Raton, FL: CRC Press)
60. Cabuk, S. & Simsek, S. Phase-separation perspective on dynamic heterogeneities in glass-forming liquids. *Phys. Scr.* **81**, 055703 (2010).
61. Kurt, M. Z. Electrooptical Properties of $LiTaO_3$. *Ferroelectrics.* **296**, 127–137 (2003).

Acknowledgements
This work was supported by the National Natural Science Foundations of China (Nos. 11104072, U1404108, 11404112, 11174220, 19ZR1459100 and 11374226), the Key scientific research projects in Colleges and Universities of Henan province (Nos. 17A140009) and Innovative Talent of University in Henan Province (17HASTIT013). We also thanks very much to Dr. Zhansheng Lu for providing assistance in calculations and to Dr. Derwyn. A. Rowlands in the polish of English.

Author contributions
Jing Zhang and San-Huang Ke designed calculational model; Bin Xu and Yu-Sheng Wang carried out calculations of electronic structures and ferroelectric properties; Jing Zhang and Zhen Qin carried out calculations of piezoelectric properties and nonlinear optical properties; Jing Zhang and San-Huang Ke analyzed the theoretical results; Jing Zhang wrote the manuscript.

Competing interests
The authors declare no competing interests.

Additional information
Correspondence and requests for materials should be addressed to J.Z.

Reprints and permissions information is available at www.nature.com/reprints.

Publisher's note Springer Nature remains neutral with regard to jurisdictional claims in published maps and institutional affiliations.